ELSEVIER

Contents lists available at ScienceDirect

Journal of Materials Science & Technology

journal homepage: www.elsevier.com/locate/jmst



Research Article

Enhanced antibacterial behavior of a novel Cu-bearing high-entropy alloy



Guangyu Ren^{a,1}, Lili Huang^{b,1}, Kunling Hu^b, Tianxin Li^a, Yiping Lu^{a,*}, Dongxu Qiao^a, Haitao Zhang^a, Dake Xu^{c,*}, Tongmin Wang^a, Tingju Li^a, Peter K. Liaw^{d,*}

- ^a Engineering Research Center of High Entropy Alloy Materials (Liaoning Province), School of Materials Science and Engineering, Dalian University of Technology, Dalian 116024, China
- ^b College of Food Science and Engineering, Ocean University of China, Qingdao 266100, China
- ^c Shenyang National Laboratory for Materials Science, Northeastern University, Shenyang 110819, China
- ^d Department of Materials Science and Engineering, The University of Tennessee, Knoxville, TN 37996, United States

ARTICLE INFO

Article history: Received 7 January 2022 Revised 23 January 2022 Available online 8 February 2022

Keywords: High-entropy alloy Antibacterial property Corrosion resistance Mechanical property

ABSTRACT

Contact infection of bacteria and viruses has been a critical threat to human health. The worldwide outbreak of COVID-19 put forward urgent requirements for the research and development of the self-antibacterial materials, especially the antibacterial alloys. Based on the concept of high-entropy alloys, the present work designed and prepared a novel Co_{0.4}FeCr_{0.9}Cu_{0.3} antibacterial high-entropy alloy with superior antibacterial properties without intricate or rigorous annealing processes, which outperform the antibacterial stainless steels. The antibacterial tests presented a 99.97% antibacterial rate against *Escherichia coli* and a 99.96% antibacterial rate against *Staphylococcus aureus* after 24 h. In contrast, the classic antibacterial copper-bearing stainless steel only performed the 71.50% and 80.84% antibacterial rate, respectively. The results of the reactive oxygen species analysis indicated that the copper ion release and the immediate contact with copper-rich phase had a synergistic effect in enhancing antibacterial properties. Moreover, this alloy exhibited excellent corrosion resistance when compared with the classic antibacterial stainless steels, and the compression test indicated the yield strength of the alloy was 1015 MPa. These findings generate fresh insights into guiding the designs of structure-function-integrated antibacterial alloys.

© 2022 Published by Elsevier Ltd on behalf of The editorial office of Journal of Materials Science & Technology.

1. Introduction

Sessile microorganisms on abiotic surfaces and the microbiologically-influenced corrosion (MIC) have caused negative effects and represented considerable costs in different fields, such as health and medical-care occupations, food processing, and home-appliance industries [1–3]. According to the US Centers for Disease Control and Prevention, *Escherichia coli (E. coli)* occupies the first place among human-related bacterial infections, and *Staphylococcus aureus (S. aureus)* takes the second position [4]. The most effective way to deal with the aforementioned challenge is to inhibit bacterial adherence and biofilm formation. In

E-mail addresses: luyiping@dlut.edu.cn (Y. Lu), xudake@mail.neu.edu.cn (D. Xu), pliaw@utk.edu (P.K. Liaw).

such a context, huge attention has been attached to antibacterial materials.

Copper (Cu) has been used for medical applications due to its essential cofactor of several enzymes and antibacterial activity [3]. Previous studies proved that the antimicrobial mechanisms of Cu ions included membrane damage [5], oxidative stress [6], and protein denaturation [7]. Significantly, these were mainly metabolismindependent mechanisms that could minimize the development of bacterial resistance. Despite its strong bactericidal effect, the main disadvantage was that the pure Cu and Cu alloys might have a Cu-burst phenomenon at the early stage when used in implant materials, resulting in pain and excessive menstrual blood loss [8]. Therefore, several types of Cu-containing stainless steels (SS), such as 316 L, 317 L, and 304 L [9-11], and Ti-Cu [12,13] alloys have been designed, which have shown reliable antibacterial activity against common pathogens. However, the aforementioned alloys require complicated heat treatments to obtain the antibacterial property, and the physical, chemical, and mechanical behavior

^{*} Corresponding authors.

¹ These authors contributed equally to this work.

of Cu-containing SS and Ti-Cu alloys are susceptible to the Cu element. For example, the plasticity and corrosion resistance of Ti-Cu alloy decrease when the Cu element is added, and the plasticity of the Ti-10Cu alloy reported in the literature [14] is only 1%. Thus, the boundedness of traditional antibacterial alloys limits its development prospects.

Since 2004, high-entropy alloys (HEAs) [15,16] have attracted considerable interest in different application scenarios due to their outstanding physical, chemical and mechanical properties [17-20]. Gradually, the integrating structures and functions of HEAs have been raised in recent years [20,21]. In 2020, Zhou et al. [22] first developed the concept of the antimicrobial HEAs (AHEAs) and designed a novel $Al_{0.4}$ CoCrCuFeNi alloy. Compared with traditional 304-Cu SS, Al_{0.4}CoCrCuFeNi performed excellent antibacterial properties in the as-cast condition. Three marine bacterial colonies on samples have significantly reduced after 1, 3, and 7 days of cultivation. Besides, Ke et al. [14] prepared a medical Ti-13Nb-13Zr-10Cu alloy that showed outstanding antibacterial behavior after 24 h of co-culture with S. aureus. Yu et al. [23] explored the antifouling abilities of AlCoCrCu_{0.5}FeNi via spark plasma sintering by taking advantage of the antimicrobial properties. The antibacterial property of Cu-HEAs on MIC applications and biomedical materials has been validated because of their higher Cu content and convenient preparation process. However, the mechanical properties and antibacterial mechanism of Cu-HEAs need to be improved and clarified.

In this study, $Co_{0.4}FeCr_{0.9}Cu_x$ (x=0.3 and 0.5) Cu-HEAs (denoted as the Cu0.3 alloy and Cu0.5 alloy, respectively) were designed and prepared. The effect of the Cu element on the microstructures, mechanical properties, corrosion resistance, and antibacterial behavior was studied systematically, and the antibacterial mechanism of Cu in HEAs was explored. The mechanical properties and antibacterial behavior of Cu-HEAs in the as-cast condition were comprehensively evaluated to verify its potential to be applied to materials for civil household appliances and medical instruments.

2. Material and methods

2.1. Alloy fabrication

The Cu-HEAs ingots were fabricated by vacuum-arc melting under a high-pure argon atmosphere. Nonequal molar ratios of commercially-pure Co, Cr, Cu (99.9 wt.%), and Fe (99.5 wt.%) were put into a water-cooled copper crucible. Each ingot was re-melted and flipped six times to ensure chemical homogeneity. The furnace chamber was first evacuated to 6×10^{-3} Pa and then backfilled with purity argon gas to reach 0.05 MPa. Microstructures and chemical compositions of HEAs were analyzed, using a field emission electron probe micro analyzer (EPMA, JEOL JXA-8530F Plus) equipped with a wavelength-dispersive spectrometer (WDS). The phase constitution of the Cu-bearing HEAs was probed by an X-ray diffractometer (XRD, PANalytical Empyrean) with a Cu-K α target and a scanning step of 4° /min.

2.2. Antibacterial assay

Antibacterial properties of the HEAs were compared with the traditional 304 SS and 304-Cu SS (3.5 wt.% Cu). The specimens used for antibacterial testing were cut from the as-cast ingots of a size, $10 \times 10 \times 2$ mm³. A schematic representation of the experiment can be viewed in the Supplementary Fig. 1. Metal coupons were subsequently put in an autoclave to sterilize at 121 °C for 20 min. Gram-negative *E. coli* and gram-positive *S. aureus* were activated by cultivation in a Luria-Bertani broth in advance at 37 °C for 18 h. Overnight cultures with a 10^5 colony-forming unit/mL

(CFU/mL) concentration in the sterile phosphate-buffered saline (PBS) were prepared. First, 1 mL of the bacterial culture was co-cultured with three coupons for each metal tested in a sterilized 24-well culture plate. Cultures containing each metal were incubated at 37 °C for 2, 6, 12, 24, and 48 h. Then, the metals were taken out and suspended in 1 mL of sterile PBS. The adhered bacteria were obtained, followed by ultrasonication for 5 min. to isolate from metal surfaces. The planktonic bacteria were removed from the remaining solutions in the 24-well plate. Planktonic bacteria and adhered bacteria were serially diluted in the sterile physiological water (0.85 wt.% NaCl). Each dilution with a volume of 100 μL was cultured on the Luria-Bertani agar plates at 37 °C for 24 h. Then, the antibacterial rates (%) were calculated as follows:

Antibacterial rate (%) =
$$(N_{ctrl} - N_{anti})/N_{ctrl} \times 100\%$$
 (1)

where $N_{\rm ctrl}$ represents the number of planktonic bacteria cocultured with 304 SS or adhered bacteria on the 304 SS surface (control), and $N_{\rm anti}$ denotes the number of planktonic bacteria cocultured with 304 SS or the number of adhered bacteria on the 304-Cu SS or HEA coupon surface.

2.3. Live and dead cell staining

The live and dead bacteria adhered to the surfaces of HEAs were stained, using a LIVE&DEAD Bacterial Staining Kit (Yisheng, Shanghai, China) in a dark environment at RT. Live bacteria with intact cell membranes were stained with green-fluorescent DMAO, and dead bacteria with damaged cell membranes were stained with red-fluorescent EthD-III. DMAO and EthD-III were mixed to observe the live (green) and dead (red) bacteria. Metals were removed from the E. coli and S. aureus suspensions after incubation at 37 °C for 6, 12, and 24 h and the samples were washed with sterile PBS to remove the nonadherent bacteria. The mixtures of DMAO and EthD-III were prepared with a volume ratio of 1:2, and then 10 μL of the mixture was added into the 24-well plate containing 1 mL of PBS and 100 μ L of bacterial suspension in the dark for 15 min. Finally, a confocal laser scanning microscope (CLSM, OLYMPUS FV3000) was used to identify the live and dead bacteria [9].

2.4. Cu-ion concentration and ROS-activity analysis

The Cu-releasing profiles from HEAs, 304 SS, and 304-Cu SS after immersion in the sterile water, *E. coli*, and *S. aureus* cultures for 2, 6, 12, 24, and 48 h were measured. After incubation, the distilled water and the bacterial suspension were collected. Then, the concentrations of the released Cu were measured by the atomic absorption spectroscopy. The ROS (H_2O_2) activity of metals was measured in this study, using a Hydrogen Peroxide Assay Kit (Solarbio, Beijing, China). All metals were immersed in 500 μ L of sterile water or sterile PBS at 37 °C. Then, the absorbance of the aforementioned solutions was measured at 415 nm via a plate reader. Each experiment was performed in triplicate.

2.5. Microbial-morphology observation

The scanning electron microscope (SEM, Zeiss Supra 55) was used to observe the *E. coli* and *S. aureus* biofilm morphologies on the surfaces of metals after being incubated for 24 h. All coupons were first fixed in a 4 vol.% glutaraldehyde solution for 4 h to immobilize the biofilm, and then the metals were dehydrated successively by ethanol solutions (25 vol.%, 50 vol.%, 75 vol.%, and 100 vol.%) for 10 min. Subsequently, the samples were subjected to freeze-drying and gold sputtering. Finally, the adhered bacteria on the HEA surface were observed by the SEM.

2.6. Electrochemical measurements, immersion experiments, and neutral salt spray tests

Corrosion resistance was measured by an electrochemical station (Gamry Reference 600) in the normal saline solution [0.9 wt.% NaCl] at 37 °C. The investigated samples were employed as the working electrode, a platinum foil as the counter electrode, and an Ag/AgCl electrode (saturated KCl with an electrode potential of 0.1981 V vs. standard hydrogen electrode) as the reference electrode. The polarization test was commenced at a scan rate of 1 mV/s after reaching a steady open circuit potential (OCP) and the potential scanning range was -1.0 - 0.7 V. The samples for immersion and neutral salt spray experiments were immersed in normal saline solution up to 7 d at 37 °C. The corrosion rate was calculated as $P_W = KW/ATD$, where P_W is the corrosion rate in mm/y, K is a constant (8.76 \times 10⁴), W is the weight loss of the sample in g, A is the surface of the sample in cm², T is the immersion time in h, and D is the density in $g \cdot cm^{-3}$. For each alloy, at least five samples were tested to obtain good statistics. Neutral salt spray tests were performed according to DIN EN ISO 9227 [21] for 168 h. Tests on five samples of each alloy were performed in a salt spray box, and the specific experimental conditions were: pH 6.8; NaCl concentration 50 g/L; deposition rate 1.6 mL/h; temperature 35 \pm 2 °C.

2.7. Mechanical testing

Room-temperature compression tests were performed, employing an Instron 5569 testing machine with a strain rate of 1×10^{-3} s $^{-1}$ at room temperature. The samples were cut into $\Phi 5\times 10$ mm directly from the ingot.

2.8. Statistics and reproducibility

The data shown as the mean \pm standard deviation (SD) was obtained by at least three independent experiments and analyzed by the GraphPad Prism software [2]. The statistical significance of observed differences was analyzed by two-way ANOVA test [2].

3. Results

3.1. Microstructure characterization

Fig. 1 shows the X-ray diffraction patterns of the Cu0.3 and Cu0.5 alloys. The XRD patterns of the as-cast Cu0.3 and Cu0.5 alloys show that both HEAs have a simple face-centered-cubic (FCC) and body-centered-cubic (BCC) structure. Fig. 2(a-d) illustrate the backscattered electron (BSE) images of the two alloys. Both alloys had a matrix phase with dispersed precipitates (indicated in

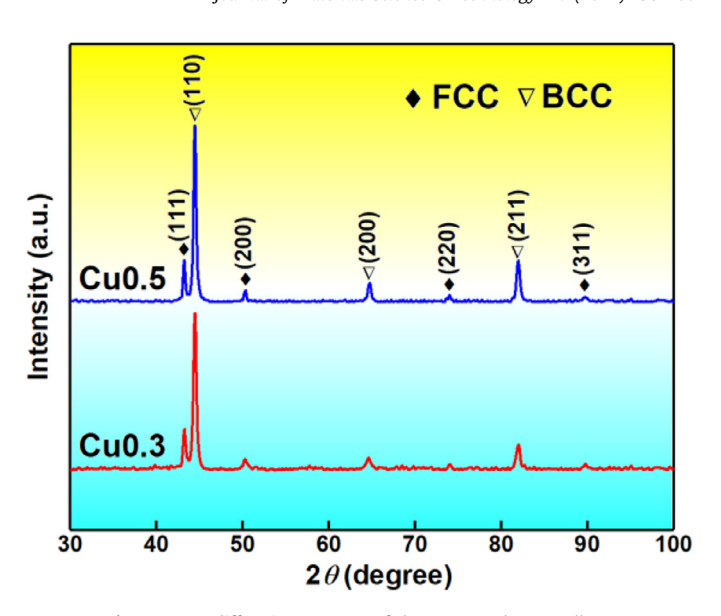


Fig. 1. X-ray diffraction patterns of the Cu0.3 and Cu0.5 alloys.

Fig. 2(b)). Through the corresponding elemental distribution images (WDS mapping) of Cu0.3 alloys (Fig. 2(e)), the regions with brighter contrast were Cu-rich phases. The Cu-rich phase and matrix contained 92 at.% and 3 at.% Cu, respectively, as presented in Supplementary Table 1. On the contrary, Co, Cr, and Fe elements were distributed in the matrix homogeneously.

3.2. In vitro antibacterial properties

The bacterial suspensions of *E. coli* and *S. aureus* were cocultured with 304 SS, 304-Cu SS, Cu0.3, and Cu0.5 alloys for 2, 6, 12, 24, and 48 h. Fig. 3 is the macroscopic picture of coupon biofilms and planktonic colonies after incubation. Significantly-fewer colonies were observed in the incubations containing Cu0.3 and Cu0.5 coupons than those containing 304 SS and 304-Cu SS. Then, the number of the planktonic bacteria surviving in the suspension and the adhered bacteria on coupons were studied, shown in Supplementary Fig. 2.

The bacterial colonies of the agar plate were separately calculated by the plate-counting method [22]. According to eq 1, the antibacterial effect of 304-Cu SS against *E. coli* and *S. aureus* was not evident until 6 h, and the antibacterial rate was 35.79% and 81.58%, respectively. The antibacterial rate of the Cu0.3 alloy against *E. coli* after 24 h was calculated to be 99.97%, and the antibacterial rate of

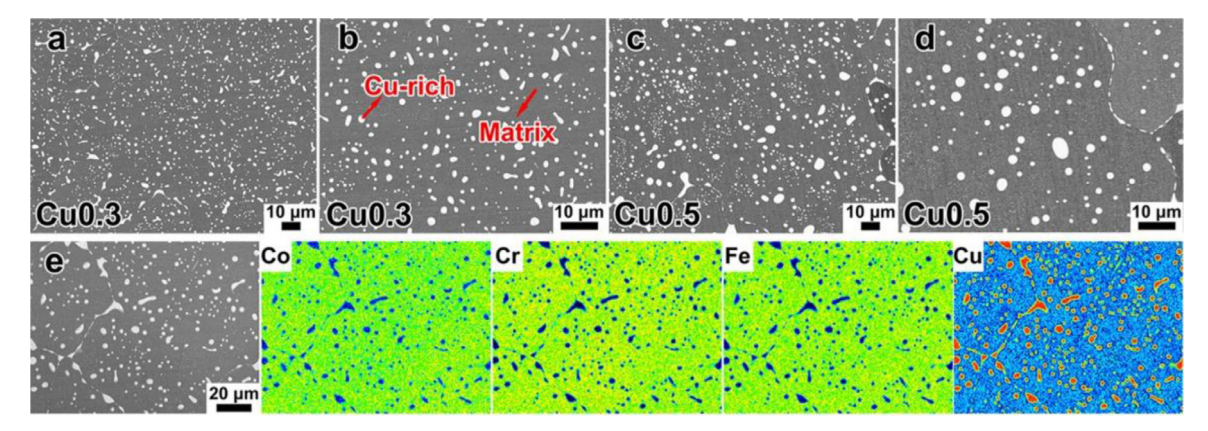


Fig. 2. SEM images and elemental mapping analysis. (a-b) Backscattered electron images of the Cu0.3 alloy. (c-d) Backscattered electron images of the Cu0.5 alloy. (e) The corresponding elemental mapping of the Cu0.3 alloy.

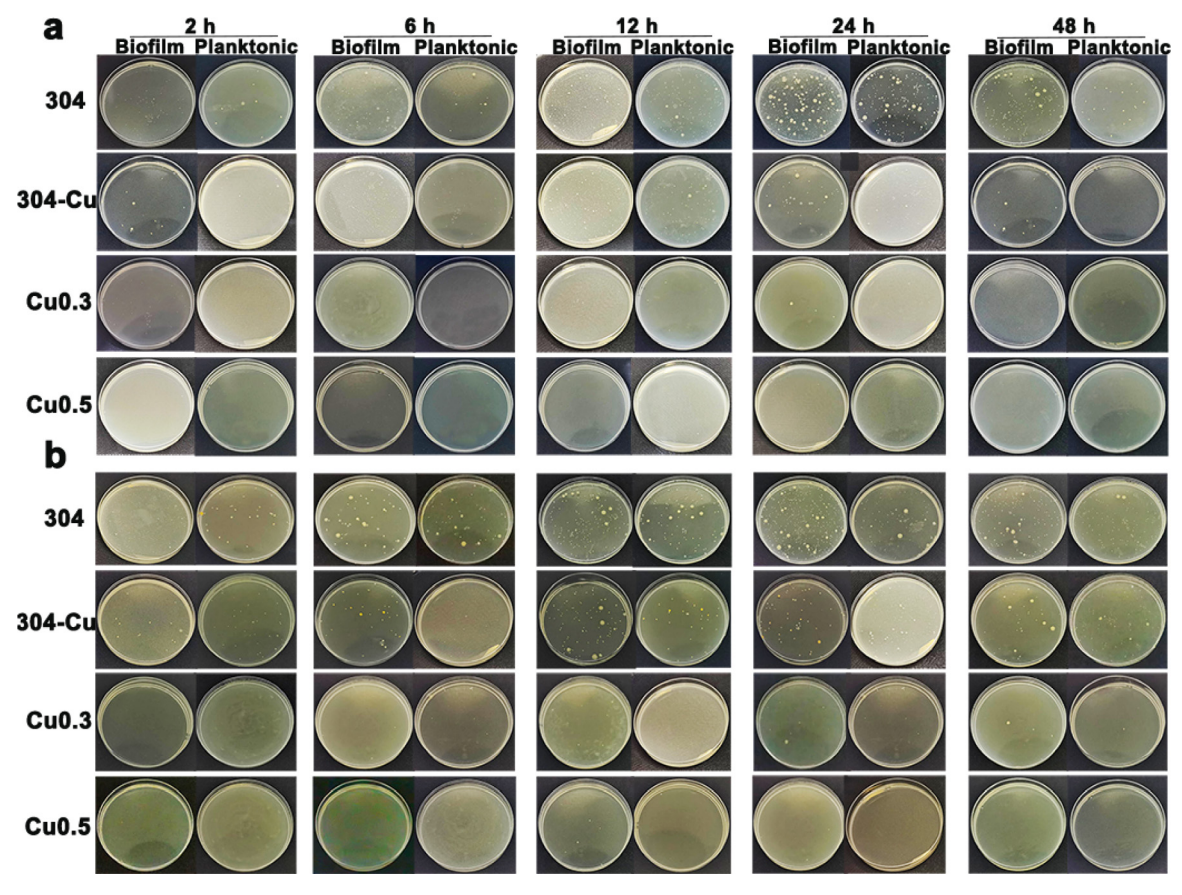


Fig. 3. The images of the bacterial colony growth after co-culture with alloys. (a) Coupon biofilm and planktonic colonies of *E. coli* after incubation for 2, 6, 12, 24, and 48 h. (b) Coupon biofilm and planktonic colonies of *S. aureus* after incubation for 2, 6, 12, 24, and 48 h.

the Cu0.3 alloy against *S. aureus* after 24 h was 99.96%, as shown in Supplementary Fig. 3. These results suggested that the novel Cu0.3 and Cu0.5 alloys serve as a long-term and broad-spectrum antibacterial agent.

The results of live/dead cell staining were seen in Fig. 4. The bacterial growth on the four different coupons after 6, 12, and 24 h was also used to study the antibacterial properties. Fig. 4(a) shows that more live E. coli (green fluorescence) were observed on the 304 SS and 304-Cu SS alloys, while more dead cells (red fluorescence) were observed on the Cu0.3 and Cu0.5 alloys after 24 h. Similar results for S. aureus indicated that both Cu0.3 and Cu0.5 alloys had an obvious bactericidal effect on these bacteria in the ascast condition. The E. coli and S. aureus cultured on samples were observed, using an SEM (Fig. 5). After 24 h of co-culture, 304 SS samples were covered by many rod-shaped and spherical bacteria, which presented as confluent colonies (Fig. 5(a), (e)). On the contrary, few colonies of E. coli and S. aureus were found on the Cu0.3 (Fig. 5(c), (g)) and Cu0.5 (Fig. 5(d), (h)) samples, and almost no complete bacterial cells were present on the aforementioned two alloys, which shows effective inhibition of the Cu0.3 and Cu0.5 alloys.

The ion-release results of the 304-Cu SS, Cu0.3, and Cu0.5 alloys were investigated to explore whether Cu ions could be released to play a bactericidal role. Fig. 6(a-c) presented the Cu ions released in the deionized (DI) water and bacterial suspension of *E. coli* and *S. aureus*. Based on the results that the Cu ions measured in the Cu0.5 alloy were all lower than that in the Cu0.3 alloy, the increased Cu element did not contribute to its release process. Fig. 6(b), (c) show that the Cu ions in the Cu0.3 and the Cu0.5 exceeded that in the 304-Cu SS at 6 h, and then reached twice as much as that in the 304-Cu SS at 12 h. The available data ex-

Table 1 Electrochemical parameters of 304 SS, 304-Cu SS, Cu0.3, and Cu0.5 alloys.

Alloys	304	304-Cu	Cu0.3	Cu0.5
$E_{\rm corr}$ (mV) $i_{\rm corr}$ (μ A/cm ²)	-153	-135	-115	-111
	2.35	2.11	2.71	2.46

plained that the significant bactericidal behavior of the Cu0.3 and Cu0.5 was directly related to the concentration of Cu ions. Compared with the Cu-releasing rate in the DI water (Fig. 6(a)), the adequate supplies of Cu ions should result from the corrosive environments in the bacterial suspension, which ensured the continuous release and contributed to the long-term sterilization.

In addition, Cu ions catalyzed oxidases and produced ROS effectively [9], which was proved to be highly toxic to most bacteria. According to Fig. 6(d), the ROS contents produced when cocultured with 304-Cu SS, Cu0.3, and Cu0.5 alloys were 0.17, 0.62, and 0.38 μ mol/mL, respectively.

3.3. Corrosion resistance and mechanical properties of the alloys

In order to study the corrosion resistance of the Cu0.3 and Cu0.5 alloys, electrochemical measurements, immersion experiments and neutral salt spray tests were carried out, as shown in Fig. 7. The potentiodynamic-polarization curves of the Cu-HEA samples indicated an increased corrosion potential after the Cu addition. Table 1 shows the corrosion potential (E_{corr}) values of Cu0.3 and Cu0.5 alloys were -115 mV and -111 mV, respectively, exhibiting a nobler corrosion potential than the 304 SS and 304-Cu SS (-153 mV and -135 mV, respectively). Meanwhile, a similar

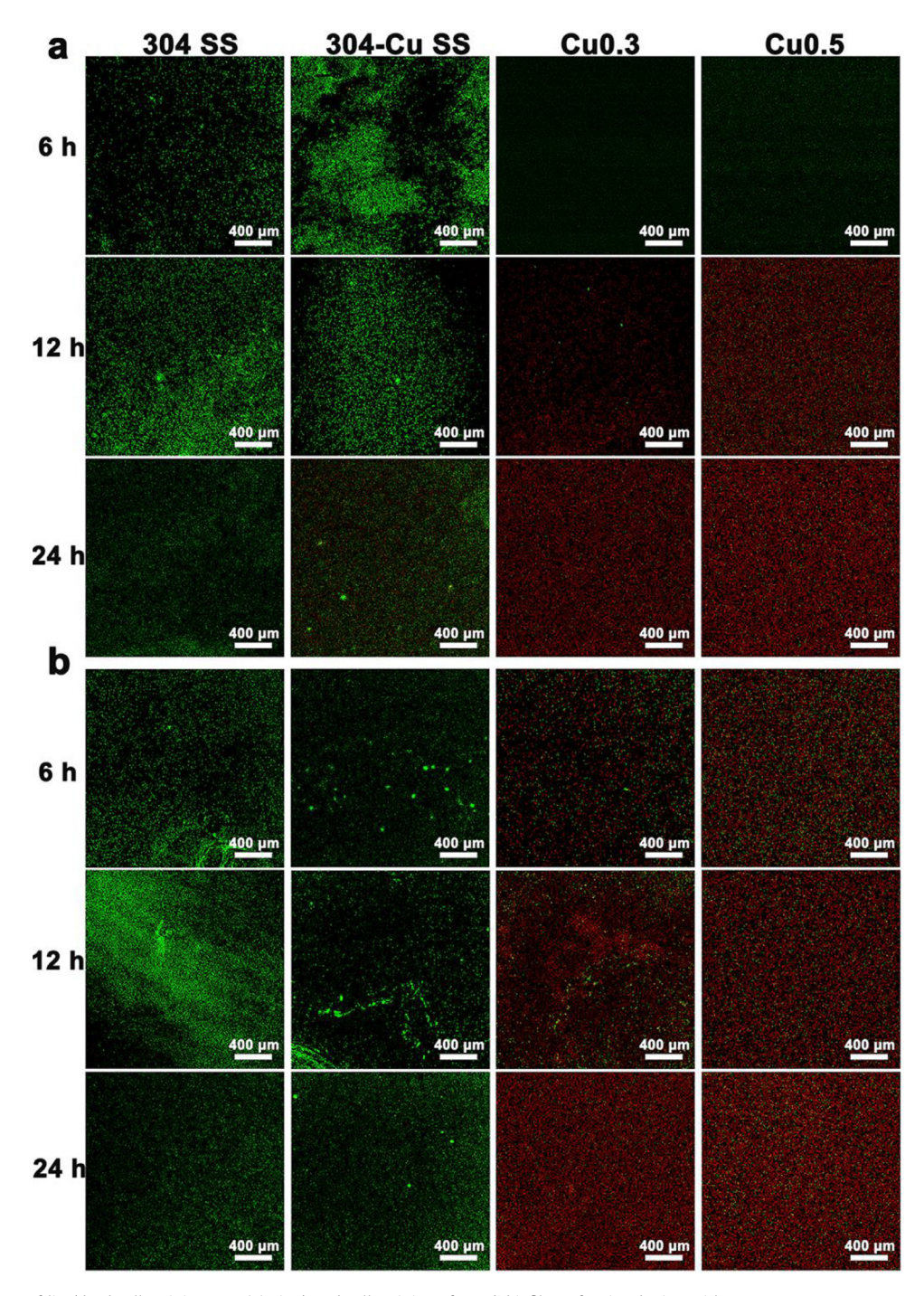


Fig. 4. The CLSM images of live/dead cell staining test. (a) Live/Dead cell staining of *E. coli* biofilms after incubation with 304 SS, 304-Cu SS, Cu0.3, and Cu0.5. (b) Live/Dead cell staining results of *S. aureus* biofilms after incubation with 304 SS, 304-Cu SS, Cu0.3, and Cu0.5 alloys.

corrosion current density ($i_{\rm corr}$) when compared with 304 SS was seen in both Cu0.3 and Cu0.5 alloys.

In addition, the corrosion rates calculated from the immersion tests were (0.0056 \pm 0.0002), (0.0048 \pm 0.0005), (0.0061 \pm 0.0003), and (0.0058 \pm 0.0003) mm/y for 304 SS, 304-Cu SS, Cu0.3, and Cu0.5 alloys, respectively. Hence, there was no significant difference in terms of the corrosion rate (as shown in Supplementary Fig. 4). Fig. 8 shows the results of the neutral salt spray tests after 7 days, the images of the alloys all had a normal silver-gray luster, and there were no obvious corrosion pits on the surfaces of the alloys. The aforementioned results amply proved that the corrosion

resistance of the present work was similar to that of the $304\ SS$ alloy.

The mechanical properties of Cu0.3 and Cu0.5 alloys were analyzed and the compression engineering stress-strain curves were shown in Fig. 9(a). The yield strength of the Cu0.3 and Cu0.5 alloys were 1015 MPa and 955 MPa, respectively, so that the present work also had advantages in specific yield strength when compared with the classic Cu-containing HEAs in mechanical response [24–38]. The comparison of the specific yield strength and plasticity between classic Cu-HEAs was displayed in Supplementary Fig. 5. What we want to emphasize here is that, although the Cu0.3

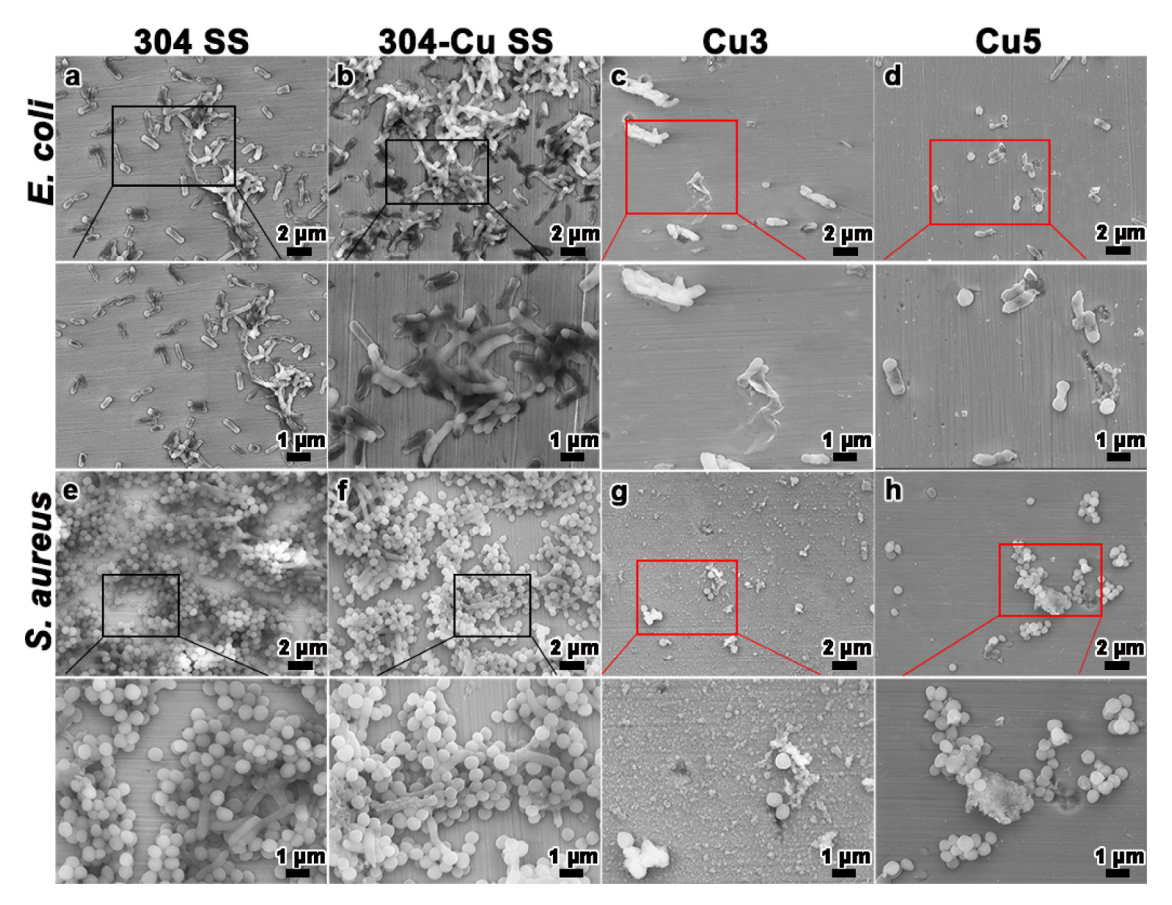


Fig. 5. The SEM images of bacteria morphology. The SEM images of (a-d) E. coli and (e-h) S. aureus cultured on 304 SS, 304-Cu SS, Cu0.3, and Cu0.5 samples after 24 h.

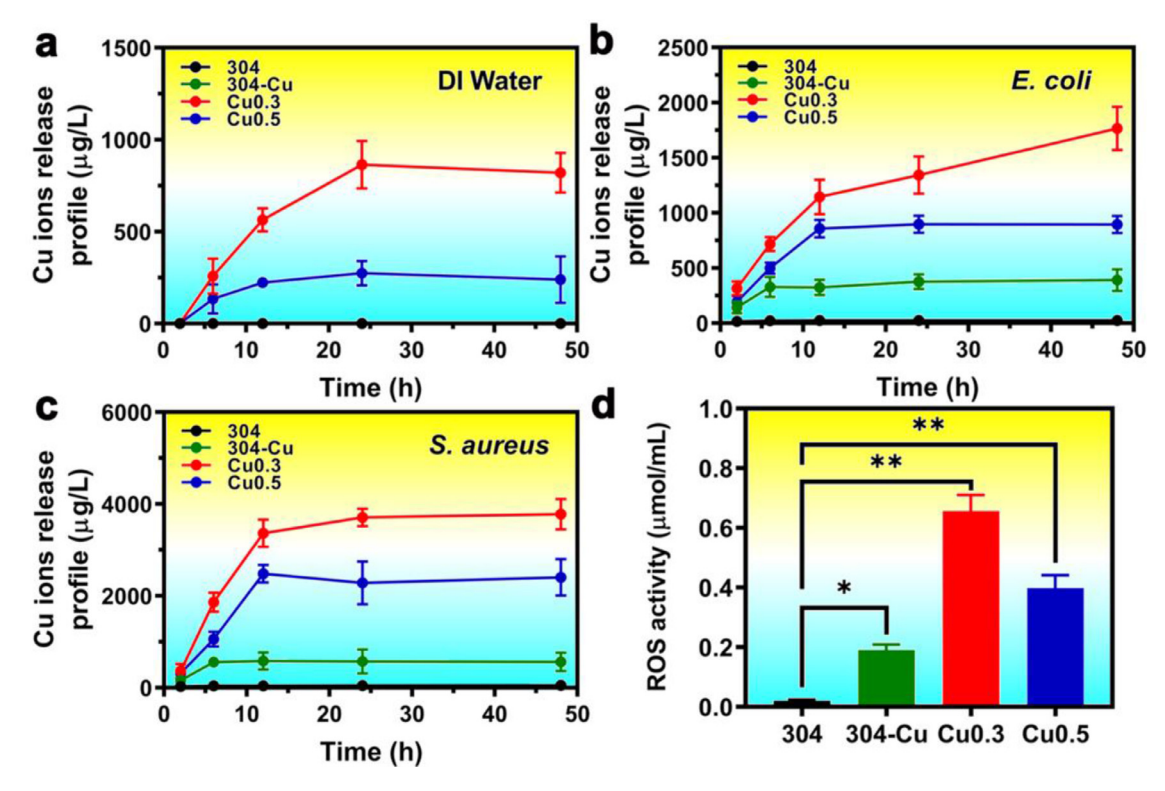


Fig. 6. The results of Cu-releasing tests, ROS activity tests, and the schematic diagram of germicidal mechanism. (a) The Cu-releasing profile in the DI water. (b) The Cu-releasing profile in bacterial suspension of *E. coli.* (c) The Cu-releasing profile in bacterial suspension of *S. aureus.* (d) ROS activity of bacterial suspension after co-culturing with 304 SS, 304-Cu SS, Cu0.3, and Cu0.5 alloys after 24 h (n = 3) (Sidak's multiple comparisons test, two-way ANOVA. 304 vs. 304-Cu, *p < 0.05; 304 vs. Cu0.3, **p < 0.001; 304 vs. Cu0.5, **p < 0.001). Data are displayed as mean \pm SD and analyzed by the GraphPad Prism software [2].

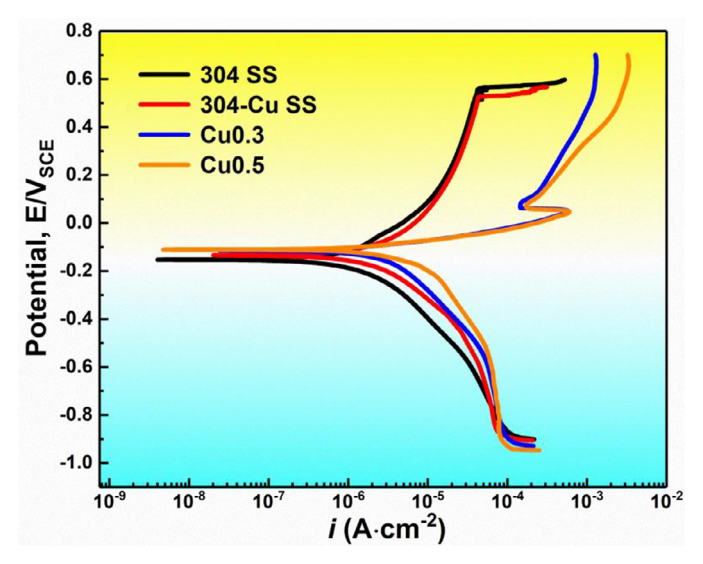


Fig. 7. The electrochemical-polarization curves of the 304 SS, 304-Cu SS, Cu0.3, and Cu0.5 alloys.

and Cu0.5 alloys in this work is not strengthened by any deformation or heat treatment, the balance of the mechanical and antibacterial properties of these as-cast alloys is still better than that of the traditional antibacterial stainless steel, as shown in Fig. 9(b).

4. Discussion

As mentioned earlier, the existence of Cu-rich precipitates and a large amount of Cu ions released in the microenvironment guaranteed the excellent bactericidal behavior of Cu-HEAs in the as-cast station. Bacterial adhesion and biofilm formation were strongly inhibited with the help of the antibacterial properties of Cu ions, and Nan et al. has confirmed the electrostatic forces of Cu²⁺ can inhibit the adhesion force of bacteria directly, then the cell walls are damaged and contents in the cells leaked [39]. The possible antibacterial mechanism in this study was discussed (Fig. 10). On the one hand, the Cu0.3 and Cu0.5 alloys were regarded as iron-based metals due to the influence of the composition element ratio. The higher standard electrode potential of Cu in the microenvironment [8] induced the formation of the Fe/Cu micro galvanic, which was

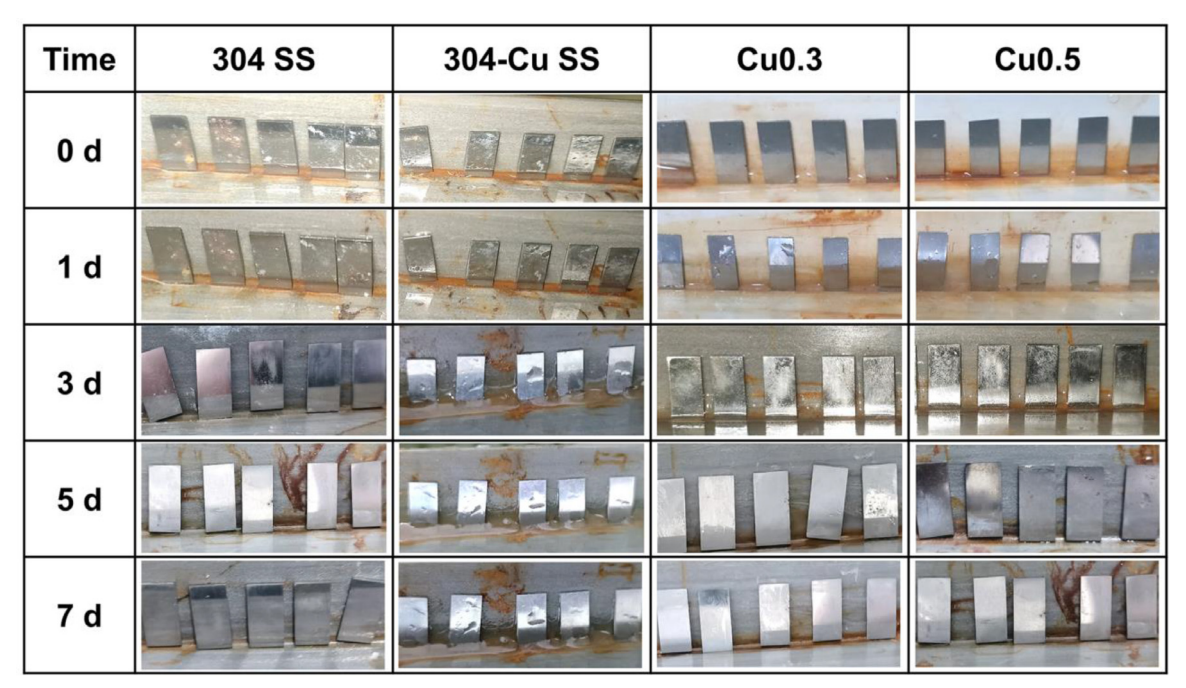


Fig. 8. Images of salt spray test of the 304 SS, 304-Cu SS, Cu0.3 and Cu0.5 alloys after 7 days.

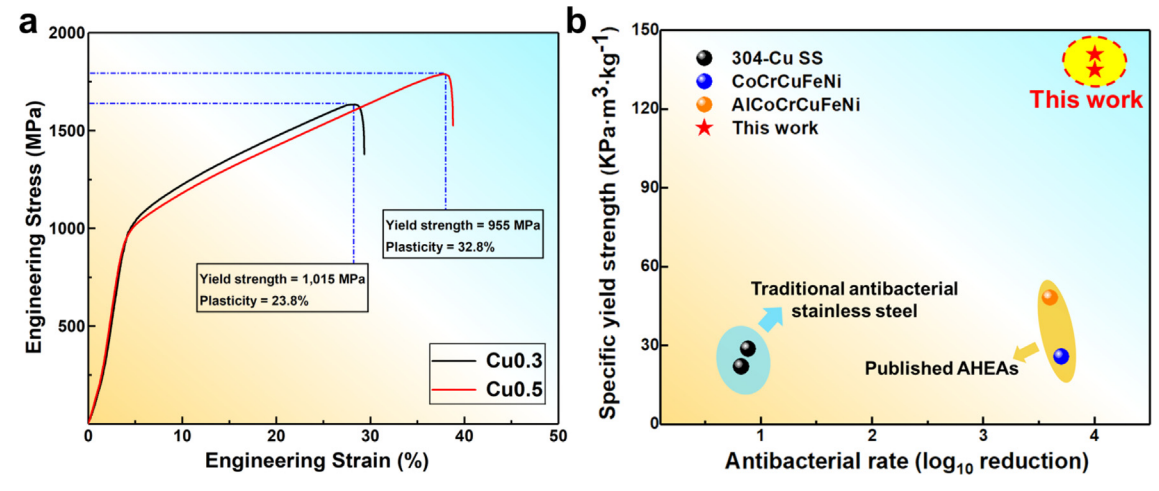


Fig. 9. The mechanical properties of the Cu-containing HEAs. (a) Compression engineering stress-strain curves of Cu0.3 and Cu0.5 alloys, and (b) the comparison of the specific yield strength and antibacterial rates between Cu-containing HEAs and the traditional antibacterial stainless steel.

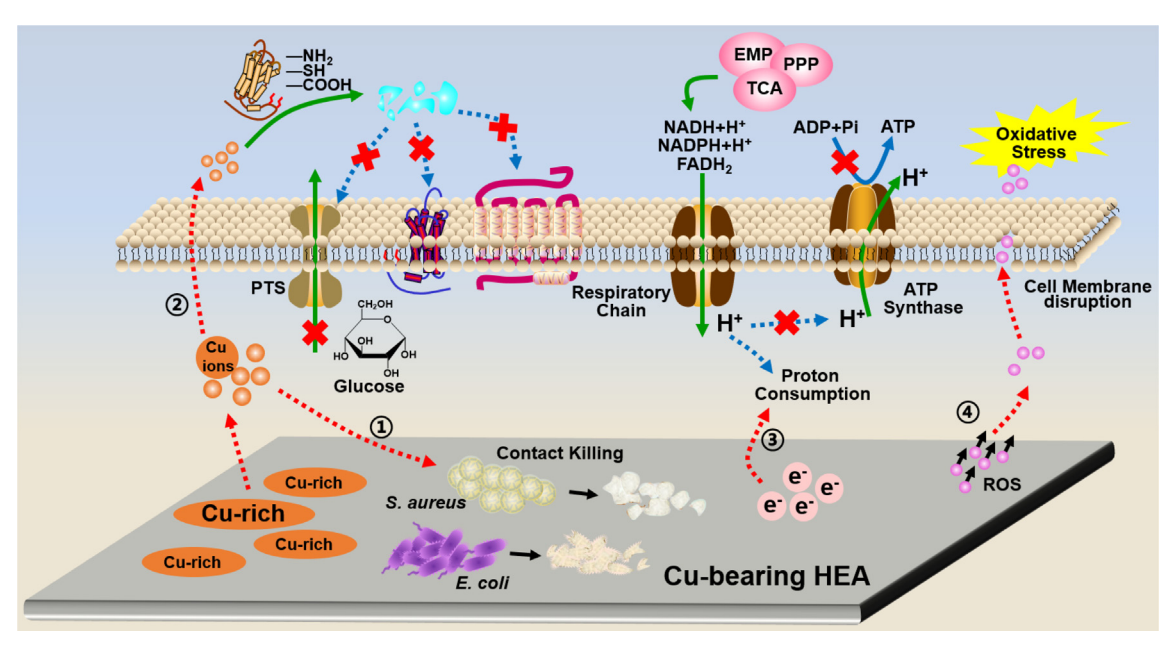


Fig. 10. The possible schematic illustration for the contact killing mechanism of Cu-HEAs. (EMP, Embden-Meyerhof-Pranas pathway; PPP, pentose phosphate pathway; TCA, tricarboxylic acid cycle; PTS, phosphotransferase system).

the cause for the massive release of copper ions [40]. Then, Cu ions play a role in contact sterilization and cause lysis and death of bacteria. On the other hand, an effective dose of ROS inspired (Fig. 6(d)) during the co-cultivation process due to the direct contact between the bacterial and the Cu-rich phase, and the ROS can induce the oxidative stress, and achieve antibacterial effect.

Moreover, the proton pump on the cell membrane continuously transfers H⁺ produced in the respiratory chain, forming a potential difference of H⁺, which can stimulate the synthesis of adenosine triphosphate (ATP) to supply energy. Zhang et al. [41] supposed that the electron produced in the microenvironment consumes the H⁺, and the proton gradient will be destroyed. So that the interruption of the ATP synthase ultimately kills the bacteria. Hence, as shown in Fig. 10, the contact killing induced by Cu ions and the proton consumption exerted a synergistic antibacterial effect, and thus the excellent broad-spectrum antibacterial properties of Cu-HEAs were confirmed.

5. Conclusions

To conclude, the present work proposed and fabricated a novel Cu-bearing AHEA and the antibacterial behavior of the alloys were investigated. In this study, the as-cast Co_{0.4}FeCr_{0.9}Cu_{0.3} alloy could achieve a high antibacterial rate without any intricate or rigorous annealing processes, which is more concise and efficient, and quite distinguished from the classic antibacterial stainless steels. With the help of Cu ions, Cu-bearing HEAs can be a promising alloy-type antimicrobial material because of the contact killing and the proton consumption mechanism, and have the potential to meet the needs of structure-function-integrated antibacterial alloys.

Declaration of Competing Interest

The authors declare no competing financial interests.

CRediT authorship contribution statement

Guangyu Ren: Conceptualization, Data curation, Formal analysis, Investigation, Writing – original draft, Writing – review & editing. **Lili Huang:** Conceptualization, Data curation, Formal analy-

sis, Writing – review & editing. **Kunling Hu:** Data curation, Formal analysis, Investigation. **Tianxin Li:** Formal analysis, Writing – original draft. **Yiping Lu:** Funding acquisition, Supervision, Project administration, Writing – review & editing. **Dongxu Qiao:** Formal analysis, Writing – original draft. **Haitao Zhang:** Formal analysis. **Dake Xu:** Funding acquisition, Supervision, Writing – review & editing. **Tongmin Wang:** Funding acquisition, Supervision, Project administration. **Tingju Li:** Funding acquisition, Supervision, Project administration. **Peter K. Liaw:** Funding acquisition, Supervision, Writing – review & editing.

Acknowledgments

Supported by the National Key Research and Development Program of China (No. 2019YFA0209901), National Natural Science Foundation of China (No. 51822402 and U20A20278), Liao Ning Revitalization Talents Program (No. XLYC1807047) and Major Special Project of "Scientific and Technological Innovation 2025" in Ningbo (No. 2019B10086). Peter K. Liaw thanks the support from the National Science Foundation (DMR-1611180 and 1809640) with the program directors, Drs. Judith Yang, Gary Shiflet, and Diana Farkas.

Supplementary materials

Supplementary material associated with this article can be found, in the online version, at doi:10.1016/j.jmst.2022.02.001.

References

- [1] R. Akid, H. Wang, T.J. Smith, D. Greenfield, J.C. Earthman, Adv. Funct. Mater. 18 (2008) 203–211.
- [2] J.Y. Xie, M. Zhou, Y.X. Qian, Z.H. Cong, S. Chen, W.J. Zhang, W.N. Jiang, C.Z. Dai, N. Shao, Z.M. Ji, J.C. Zou, X.M. Xiao, L.Q. Liu, M.Z. Chen, J. Li, R.H. Liu, Nat. Commun. 12 (2021) 5898.
- [3] T.M. Gross, J. Lahiri, A. Golas, J. Luo, F. Verrier, J.L. Kurzejewski, D.E. Baker, J. Wang, P.F. Novak, M.J. Snyder, Nat. Commun. 10 (2019) 1979.
- [4] W.X. Xi, V. Hegde, S.D. Zöller, H.Y. Park, C.M. Hart, T. Kondo, C.D. Hamad, Y. Hu, A.H. Loftin, D.O. Johansen, Z. Burke, S. Clarkson, C. Ishmael, K. Hori, Z. Mamouei, H. Okawa, I. Nishimura, N.M. Bernthal, T. Segura, Nat. Commun. 12 (2021) 5473.
- [5] H.L. Karlsson, P. Cronholm, Y. Hedberg, M. Tornberg, L. De Battice, S. Svedhem, I.O. Wallirider, Toxicology 313 (2013) 59–69.

- [6] K.S. Chaturvedi, J.P. Henderson, Front. Cell. Infect. Microbiol. 4 (2014) 1-12.
- [7] M. Vincent, R.E. Duval, P. Hartemann, M. Engels-Deutsch , J. Appl. Microbiol. 124 (2018) 1032-1046.
- [8] S.A. Yavari, S.M. Castenmiller, J.A.G. van Strijp, M. Croes, Adv. Mater. 32 (2020) 2002962.
- [9] Y.F. Zhuang, S.Y. Zhang, K. Yang, L. Ren, K.R. Dai , J. Biomed. Mater. Res. Part B 108 (2020) 484–495.
- [10] D. Sun, D.K. Xu, C.G. Yang, J. Chen, M.B. Shahzad, Z.Q. Sun, J.L. Zhao, T.Y. Gu, K. Yang, G.X. Wang, Mater. Sci. Eng. C 69 (2016) 744–750.

 [11] L. Nan, D.K. Xu, T.Y. Gu, X. Song, K. Yang, Mater. Sci. Eng. C 48 (2015) 228–234.
- [12] Z. Ma, M. Li, R. Liu, L. Ren, Y. Zhang, H.B. Pan, Y. Zhao, K. Yang, J. Mater. Sci. 27 (2016) 91.
- [13] B. Bai, E.L. Zhang, J.C. Liu, J.T. Zhu, Dent. Mater. J. 35 (2016) 659-667.
- [14] Z.Y. Ke, C.B. Yi, L. Zhang, Z.Y. He, J. Tan, Y.H. Jiang, Mater. Lett. 253 (2019) 335-338
- [15] J.W. Yeh, S.K. Chen, S.J. Lin, J.Y. Gan, T.S. Chin, T.T. Shun, C.H. Tsau, S.Y. Chang, Adv. Eng. Mater. 6 (2004) 299-303.
- [16] B. Cantor, I.T.H. Chang, P. Knight, A.J.B. Vincent , Mater. Sci. Eng. A 375 (2004) 213 - 218.
- [17] S.L. Wei, S.J. Kim, J.Y. Kang, Y. Zhang, Y.J. Zhang, T. Furuhara, E.S. Park, C.C. Tasan, Nat. Mater. 19 (2020) 1175-1181.
- [18] W.D. Li, D. Xie, D.Y. Li, Y. Zhang, Y.F. Gao, P.K. Liaw , Prog. Mater. Sci. 118 (2021) 100777
- [19] Z.M. Li, K.G. Pradeep, Y. Deng, D. Raabe, C.C. Tasan, Nature 534 (2016) 227.
- [20] Y. Zhang, T.T. Zuo, Z. Tang, M.C. Gao, K.A. Dahmen, P.K. Liaw, Z.P. Lu, Prog. Mater. Sci. 61 (2014) 1-93.
- [21] DIN EN ISO 9227, in: Corrosion Tests in Artificial Atmospheres-Salt Spray Tests, Deutsches Institut für Normung e.V. (DIN), 2006, pp. 1-24.
- [22] E.Z. Zhou, D.X. Qiao, Y. Yang, D.K. Xu, Y.P. Lu, J.J. Wang, J.A. Smith, H.B. Li, H.L. Zhao, P.K. Liaw, F.H. Wang, J. Mater. Sci. Technol. 46 (2020) 201-210.
- [23] Y. Yu, N.N. Xu, S.Y. Zhu, Z.H. Qiao, J.B. Zhang, J. Yang, W.M. Liu, J. Mater. Sci.

- Technol. 69 (2021) 48-59.
- [24] H.T. Zhang, K.W. Siu, W.B. Liao, Q. Wang, Y. Yang, Y. Lu, Mater. Res. Express 3 (2016) 094002.
- [25] A. Verma, P. Tarate, A.C. Abhyankar, M.R. Mohape, D.S. Gowtam, V.P. Deshmukh, T. Shanmugasundaram, Scr. Mater. 161 (2019) 28-31.
- [26] J.F. Jiang, M.J. Huang, Y. Wang, G.F. Xiao, Y.Z. Liu, Y. Zhang, J. Alloy Compd. 876 (2021) 160102.
- [27] H.J. Wang, Z.Y. Wu, H. Wu, H.G. Zhu, W.C. Tang, Trans. Indian Inst. Met. 74 (2021) 267-272.
- [28] Y.K. Kim, B.J. Lee, S.K. Hong, S.I. Hong, Mater. Sci. Eng. A 781 (2020) 139241.
- [29] X.F. Wang, Y. Zhang, Y. Qiao, G.L. Chen , Intermetallics 15 (2007) 357–362.[30] S.M. Oh, S.I. Hong , Mater. Chem. Phys. 210 (2018) 120–125.
- [31] A. Shabani, M.R. Toroghinejad, A. Shafyei, R.E. Loge , J. Mater. Eng. Perform. 28 (2019) 2388-2398.
- [32] H. Qiu, H.G. Zhu, J.F. Zhang, Z.H. Xie , Mater. Sci. Eng. A 769 (2020) 138514.
 [33] S. Samal, S. Mohanty, A.K. Mishra, K. Biswas, B. Govind , Mater. Sci. Forum 790-791 (2014) 503-508.
- [34] C.J. Tong, Y.L. Chen, S.K. Chen, J.W. Yeh, T.T. Shun, C.H. Tsau, S.J. Lin, S.Y. Chang Metall. Mater. Trans. A 36 (2005) 881–893.
- [35] A.V. Kuznetsov, D.G. Shaysultanov, N.D. Stepanov, G.A. Salishchev, O.N. Senkov Mater. Sci. Eng. A 533 (2012) 107-118.
- [36] N. Deng, J. Wang, J.X. Wang, Y.X. He, Z.Y. Lan, R.F. Zhao, E. Beaugon, J.S. Li, Mater. Lett. 285 (2021) 129182.
- [37] C. Liu, W.Y. Peng, C.S. Jiang, H.M. Guo, J. Tao, X.H. Deng, Z.X. Chen , J. Mater. Sci. Technol. 35 (2019) 1175-1183.
- [38] J.H. Pi, Y. Pan, H. Zhang, L. Zhang, Mater. Sci. Eng. A 534 (2012) 228–233.
- [39] L. Nan, Y.Q. Liu, M.Q. Lu, K. Yang , J. Mater. Sci. Mater. Med. 19 (2008) 3057-3062.
- [40] H.Y. Zhao, Y.P. Sun, L. Yin, Z. Yuan, Y.L. Lan, D.K. Xu, C.G. Yang, K. Yang, J. Mater. Sci. Technol. 66 (2021) 112-120.
- [41] X.R. Zhang, C.G. Yang, K. Yang, ACS Appl. Mater. Interfaces 12 (2020) 361–372.